

PROGRESSION OF STREAMBANK EROSION DURING A LARGE FLOOD, RIO PUERCO ARROYO, NEW MEXICO

Eleanor R. Griffin, Hydrologist, U.S. Geological Survey, Boulder, CO, egriffin@usgs.gov; J. Dungan Smith, Hydrologist, U.S. Geological Survey, Boulder, CO, jdsmith@usgs.gov; Jonathan M. Friedman, Riparian Ecologist, U.S. Geological Survey, Fort Collins, CO, friedmanj@usgs.gov; Kirk R. Vincent, Geomorphologist, Boulder, CO, kvincent28@mac.com

Abstract

In August 2006, a large flood following saltcedar control efforts through a 12-km long segment of the Rio Puerco arroyo resulted in extensive lateral erosion of the streambanks. Almost all woody vegetation on the floodplain and channel banks had been killed by aerial spraying with herbicide in September 2003. During the flood, dead woody bank stems were either removed by the >4-m-deep flood flow or flattened against the bank, eliminating the source of drag that would have protected the banks from erosion. Owing to downstream variation in the shear stresses on the channel banks and floodplain, lateral erosion of the channel banks was highly variable within the sprayed reach, but channel width increased by an average of 84%. Locations and magnitudes of channel bank erosion were documented from high-resolution imagery and a post-flood (January 2007) high-precision Global Positioning System survey. Topographic data collected during the January 2007 field survey combined with geomorphic mapping from imagery provided a means to infer the progression and relative timing of bank erosion during the flood. Observations and calculations indicate channel widening resulted from a combination of direct fluvial erosion of the lower banks and mass failures of the upper banks. Applications of physically based models of flow and sediment transport demonstrate the relative influence of local floodplain slope, arroyo topography, and orientation of the channel centerline relative to the down-valley axis on bank erosion. Differences in suspended sand concentrations computed using model-calculated “skin friction” shear stress quantify the erosion rate at a site where channel width doubled during the flood.

INTRODUCTION

Background

The Rio Puerco is an ephemeral tributary of the Rio Grande that flows within an arroyo incised in fine-grained valley-fill sediments. Runoff within the 19,030-km² watershed area is largely unregulated, and the drainage area contributing runoff to the lower Rio Puerco totals 16,100 km². This area includes uplands of north-central New Mexico. The Rio Puerco is the principal source of sediment to the Middle Rio Grande and Elephant Butte Reservoir (Bryan and Post, 1927; Love, 1986). The lower Rio Puerco begins at the confluence with the Rio San Jose (Figure 1) and extends 70 km down-valley to the confluence with the Rio Grande near Bernardo.

Recent efforts to control invasive riparian species, including saltcedar (*Tamarix* spp.), have been implemented in order to increase available water supply and restore native habitat (Shafroth et al., 2005; Cleverly et al., 2006; Wilcox et al., 2006). Costly projects (e.g., Barz et al., 2009) have included large-scale applications of physical, chemical, or biological methods to remove these species. Saltcedar is the dominant riparian species along the lower Rio Puerco, and in September 2003, a 12-km long segment of the arroyo was sprayed by helicopter with herbicide (Figure 1), killing almost all woody vegetation on the floodplain and channel banks (Vincent et al., 2009). A large flood in August 2006 resulted in extensive lateral erosion of the channel banks within the sprayed reach and deposition of sand on the floodplain downstream from sites of erosion. Channel width increased by an average 84% through the sprayed reach, whereas upstream and downstream from the sprayed reach, channel banks remained intact, protected by the presence of healthy woody vegetation, including saltcedar and willow (*Salix* spp.).

Smith (2007) distinguishes between geomorphic change owing to floodplain surface erosion and bank erosion. While he focused on quantifying the former, this paper focuses on quantifying the latter. Specifically, the purpose of this work was to apply physically based models of flow and sediment transport to gain an understanding of the processes resulting in the observed lateral erosion of the channel banks during a relatively short-duration (14-hour) flood event. In the system studied by Smith (2007) as well as the Rio Puerco arroyo, channel bed and banks are composed of fine sediment. In the Rio Puerco, sediment is dominantly fine to very fine sand. As a result, the dominant mode of sediment transport in the Rio Puerco is as suspended load.

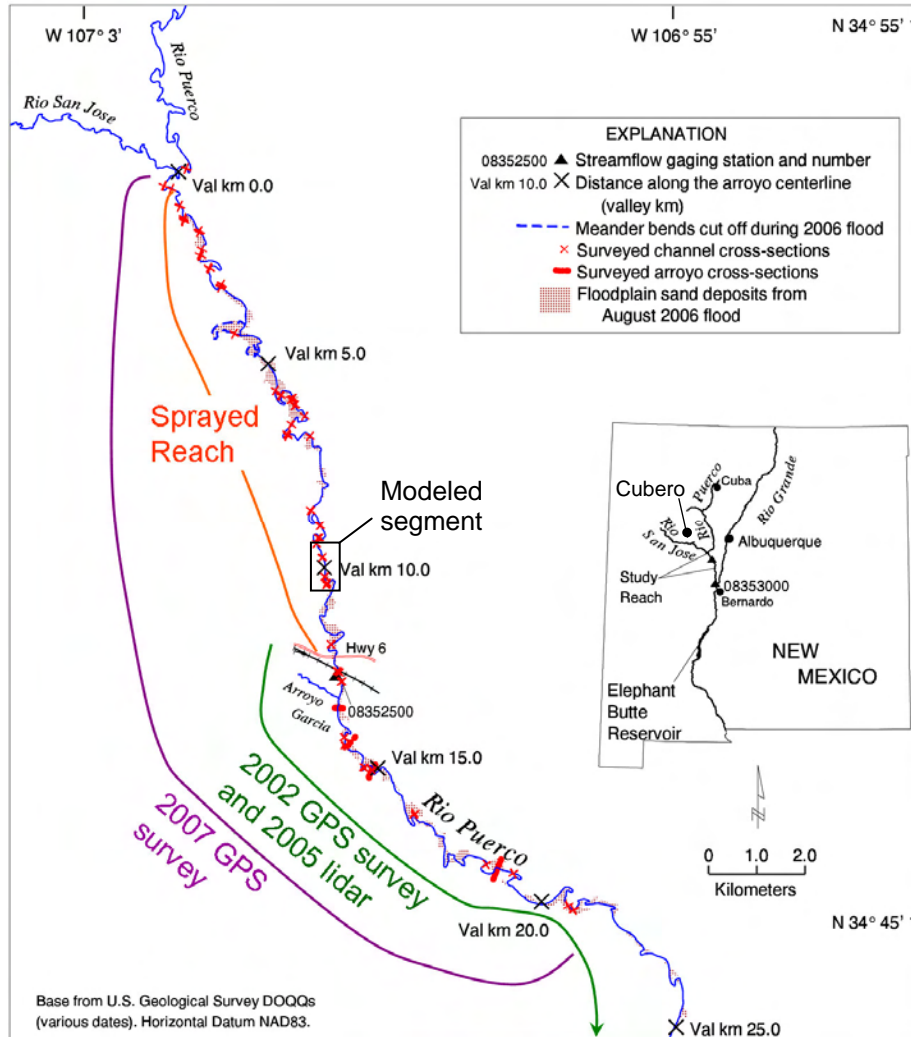


Figure 1. The study reach extends 22 km down-valley along the arroyo centerline from the confluence with the Rio San Jose. The sprayed reach begins 0.5 km down-valley from the confluence and ends at the Highway 6 (Hwy 6) bridge, 11.9 km down-valley from the confluence. The location of the modeled channel segment within the sprayed reach is indicated by the box. (Modified from Vincent et al., 2009).

Precipitation and Runoff

Daily convective thunderstorms resulting from “a remarkably persistent monsoon regime” over central and western New Mexico during the first week of August 2006 (National Weather Service (NWS) Weather Forecast Office, Albuquerque, 2006) produced record rainfall over the central Rio Puerco watershed. Daily precipitation estimates for the watershed derived from radar, rain gauge, and satellite data (NWS Advanced Hydrologic Prediction Service (AHPS), 2006) provide an indication of both the extent and intensity of rainfall throughout the watershed. Daily estimates for the period August 3 - 9 suggest the heaviest precipitation fell over the central area of the watershed, including areas draining into the Rio San Jose and the Middle Rio Puerco, upstream from the confluence with the Rio San Jose. Although only 4 NWS climate stations are located within this sparsely populated watershed, news reports of locally heavy precipitation and flooding provide additional information about precipitation timing, extent, and intensity.

During the 10-day period leading up to the peak flood flow recorded at the gaging station near Bernardo on August 10, 2006, the largest precipitation totals recorded within the watershed were reported by the climate station located at Cubero (station number 292250; Figure 1). Average annual precipitation at this station is 11.0” (279 mm). Daily

climate record totals (National Climate Data Center, 2006; Figure 2) on August 3rd, 6th, and 7th contributed to the highest total precipitation recorded at this station during the month of August, 6.40" (163 mm), throughout the 39-year period of record (Western Regional Climate Center, 2009). Also, the Gallup Independent reported that a slow-moving thunderstorm in the vicinity of Cubero on the night of August 3-4, 2006, flooded roads through Cubero and caused about \$1 million in damage to an interstate highway exit ramp (Tiffin, 2006).

Repeated daily intense thunderstorms over the Rio Puerco watershed saturated the landscape, resulting in rapid runoff accumulation in the lower Rio Puerco from August 4 – 11, 2006 (Figure 2). Streamflow recorded at Bernardo exceeded the bankfull discharge during smaller peak flows August 4-5 and 7-9, contributing to the August 10 flood peak by reducing available overbank storage volume in floodplain topographic depressions. The peak flood flow arrived at the streamflow-gaging station near Bernardo at about 0500 hours MST on August 10, 2006, and the nearly steady peak flow lasted about 14 hours at that location. The 176 m³/s flood peak discharge at Bernardo was the largest peak discharge recorded at that location since 1972 (U.S. Geological Survey, National Water Information System (NWISWeb), <http://waterdata.usgs.gov/nwis>).

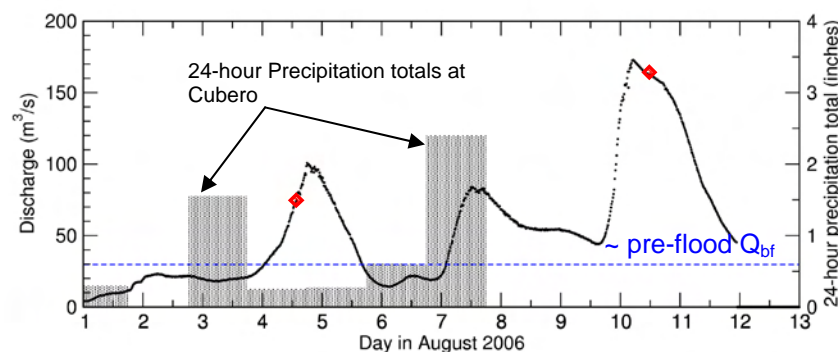


Figure 2. Discharge determined from the record of the USGS streamflow-gaging station Rio Puerco near Bernardo, New Mexico (black dotted line) and 24-hour precipitation totals measured at the climate station near Cubero. The blue dashed line represents bankfull discharge (Q_{bf}) in the vicinity of Hwy 6, and red diamonds indicate discharge determined from direct measurements made near the gaging station. Suspended sediment samples were collected along with the discharge measurements.

Observed Bank Erosion

Following the August 2006 Rio Puerco flood, extensive bank erosion was observed in the sprayed reach within both straight channel segments and meanders. About 62% of the total bank length in the sprayed reach eroded, and channel width increased from an average of 12.7 m in 2005 to 23.4 m in November 2006 (Vincent et al., 2009). Upstream and downstream from the sprayed reach, channel banks remained intact, with erosion observed only at locations where the channel was actively cutting into the arroyo wall. Increases in channel width were mapped using pre- and post-flood high-resolution imagery. Post-flood channel shape in the sprayed reach was surveyed using high-precision, real-time kinematic (RTK) Global Positioning System (GPS) equipment in January 2007.

High-precision GPS data from the January 2007 field survey (Vincent et al., 2009) indicate that the extent of lateral bank erosion was highly variable, ranging from little-to-no bank erosion to more than doubling of the channel width in many locations. The large variability in post-flood width demonstrates that the duration of the peak flood flow, about 14 hours, was not sufficient to produce an equilibrium high-flow hydraulic geometry in the sprayed reach. Geomorphic characteristics at sites of observed bank erosion were highly variable and were not always consistent with expected erosional settings. For example, some straight channel segments several hundred meters in length more than doubled in width, while in others there was little evidence of bank erosion. Erosion is expected at the apexes of meanders, but along the outside bank at several meanders little erosion was observed after the flood. This paper quantitatively examines some of the reasons for this variability.

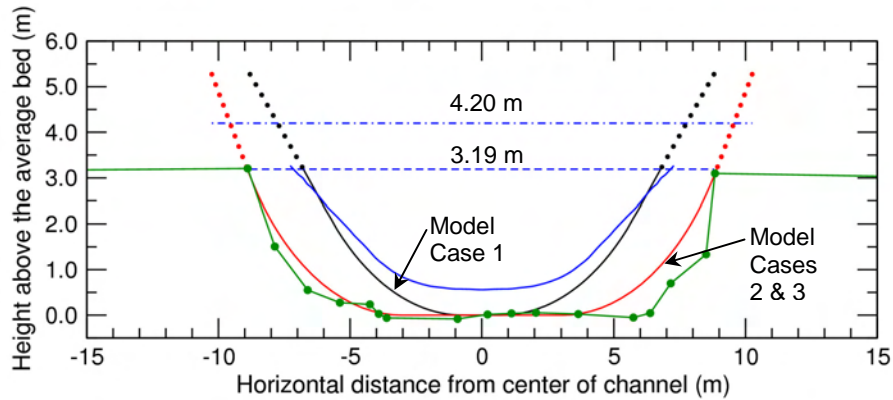


Figure 3. Rio Puerco reach-averaged channel shape prior to the flood (solid blue line); early in the flood, prior to bank erosion (black line); and after 4 m of lateral bank erosion (red line), with banks extrapolated up to the water surface (dotted lines). The green line provides an example of a single post-flood cross-section where bank erosion widened the channel.

MODEL INPUT PARAMETERS

Modeled Channel Shapes

Modeled channel shapes were derived from the January 2007 field survey data and a reach-averaged shape for the first 27 river km downstream from Hwy 6 previously derived from April 2002 GPS survey data (Griffin et al., 2005). The estimated average pre-flood channel in the sprayed reach (Figure 3) had a bankfull depth of 2.63 m, top width of about 14 m and an average bank angle of 32° . Average radius of curvature of the bank toe in the vertical cross-stream plane was about 10 m prior to the flood. Comparison of post-flood surveyed cross-sections suggests the channel bed at the modeled location eroded to a depth of about 0.56 m, increasing the bankfull depth to 3.19 m (Table 1). Calculations indicate the volume of sediment eroded from the bed that produces 0.56 m of scour (assuming 35% porosity in the bed) results in a vertically averaged volume concentration of 11% in the flood flow. Sediment eroded from the bed was likely carried into suspension during the rising limb of the flood flow. The fraction of the wetted perimeter identified as the active channel bed (for sediment transport modeling) is that part of the boundary below the middle of the rounded corner. For the early flood channel shape, 44% of the perimeter was below the middle of the corner at a height of 0.51 m (Figure 3; Table 1). In the widened channel (eroded banks shape), the active bed was the 60% of the perimeter below a height of 0.61 m.

For the somewhat cohesive upper banks to erode by mass failure at the same rate as the toe, the upper banks had to steepen and the radius of curvature of the basal part of the bank had to decrease. For the degree of cohesion in the upper banks of the Rio Puerco through this reach, these adjustments led to a reach-averaged measured upper bank slope of 45.7° and a 7.0-m calculated radius of curvature (black line in Figure 3). The 7.0-m radius of curvature results in a monotonically decreasing boundary shear stress toward the center of the channel (Figure 4A), so that sand eroded from the channel banks becomes mixed uniformly across the channel. As shown in Figure 4, a smaller radius of curvature at the bank toe results in a dip in the boundary shear stress at that location. This dip causes a reduction in the sediment transport and, hence, deposition until the radius of curvature increases, unless the sediment flux from the upper bank is restricted by form drag on plants, cohesion, or decreasing shear stress.

Table 1. Modeled channel bankfull shape parameters.

Channel Shape	Bankfull depth (m)	Top width (m)	XS area (m ²)	Hydraulic radius (m)	Average depth (m)	Width/average depth	Bed fraction of perimeter
Early flood (Case 1)	3.19	13.6	31.1	1.99	2.30	5.9	0.44
Eroded banks (Cases 2 & 3)	3.19	17.8	45.7	2.29	2.57	6.9	0.60

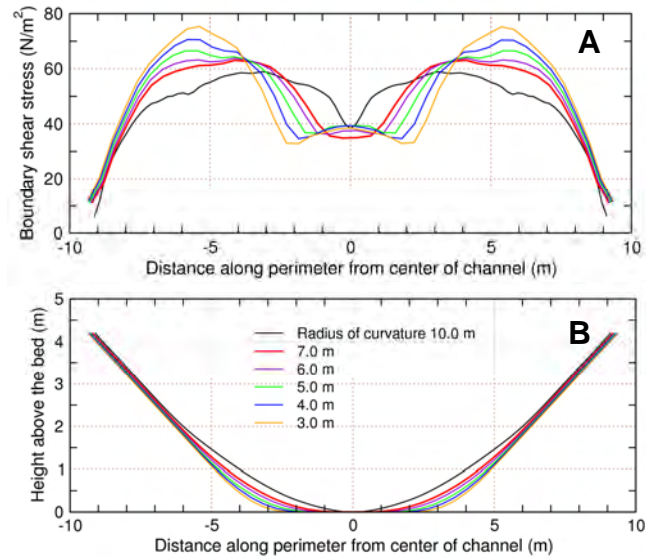


Figure 4. Model-calculated boundary shear stress distribution (A) as a function of varying radius of curvature at the bank toe (B). Modeled flow stage is 4.2 m, slope is the reach average determined from the surveyed high-water marks, 0.0021, and top width is 15.5 m in all cases. Note that small changes in the reach-averaged channel cross-section shape can have a large effect on the cross-stream distribution of boundary shear stress.

Field data indicate fluvial erosion of the lower banks during the flood and relatively small-scale mass failures along the somewhat cohesive upper banks further steepened the upper banks to an average angle of 57° (red line in Figure 3). Channel cross-sections surveyed in January 2007 suggest that erosion following the peak flood flow reduced the radius of curvature at the bank toe to the minimum (3.0 m) shown in Figure 4. As shown in Figure 4, a consequence of steepening the banks as the channel widened was a reduction in the boundary shear stress at the bank toe and a resulting reduction in the erosion rate. As a consequence of the high boundary shear stress on the upper bank, even with the form drag of the bank irregularities removed, there may have been some direct erosion of sediment from the channel banks.

Planform Geometry and Longitudinal Profiles

Bank erosion did not always occur at expected sites. The magnitude of the peak flood flow, which was on average 1-m-deep above the tops of the banks throughout the study reach, together with the geomorphic setting of the channel within the confining arroyo walls (Figure 5A) combined to influence the magnitude of local bank erosion. The orientation of the channel centerline (i.e., center of the bankfull water surface) relative to the down-valley axis affected the local water-surface slope, in some cases reducing the boundary shear stress from that expected at the apexes of sharp bends or locally increasing the shear stress along straight channel segments.

Floodplain topography prior to the August 2006 flood that resulted from shallow overbank flows since 1972 (Vincent et al., 2009) included steep drops down-valley across floodplain surfaces at bends, as shown in Figure 5C. A single flood high-water mark was surveyed within this reach in January 2007. Therefore, the flood-flow water-surface slope was estimated from the local floodplain slope and the bed gradient determined from average bed elevations at the surveyed cross-sections. Average bed elevations provide an indication of water-surface slope during the peak flood flow, whereas the January 2007 reach-average thalweg gradient, 0.0011, reflects minor erosion and rearrangement of the bed following the flood flow.

A divergence in the boundary shear stress is required to either erode sand (by increasing shear stress) or deposit sand already in suspension (by decreasing shear stress). Approaching cross-section 82, the down-valley flow over the floodplain converged with the downstream flow in the channel and the floodplain slope decreased, decreasing the boundary shear stress and forcing the deposition of sand in suspension. From cross-section 82 to mid-way between cross-sections 83 and 84, the floodplain slope (0.0021) was the same as the average slope determined from the

surveyed high-water marks in the sprayed reach. Downstream from this point, survey data indicate both the downstream channel bed slope (5B) and the down-valley (5C) floodplain slope decreased to 0.0006, possibly due to a backwater condition created by the exceptionally narrow floodplain in this segment and curvature of the arroyo bottom superimposed on channel curvature in the vicinity of cross-section 85. In the vicinity of cross-section 84, both the floodplain and average bed slopes increased to about 0.0015. Potential bank erosion rates at the site of increasing slope (and boundary shear stress) are examined below.

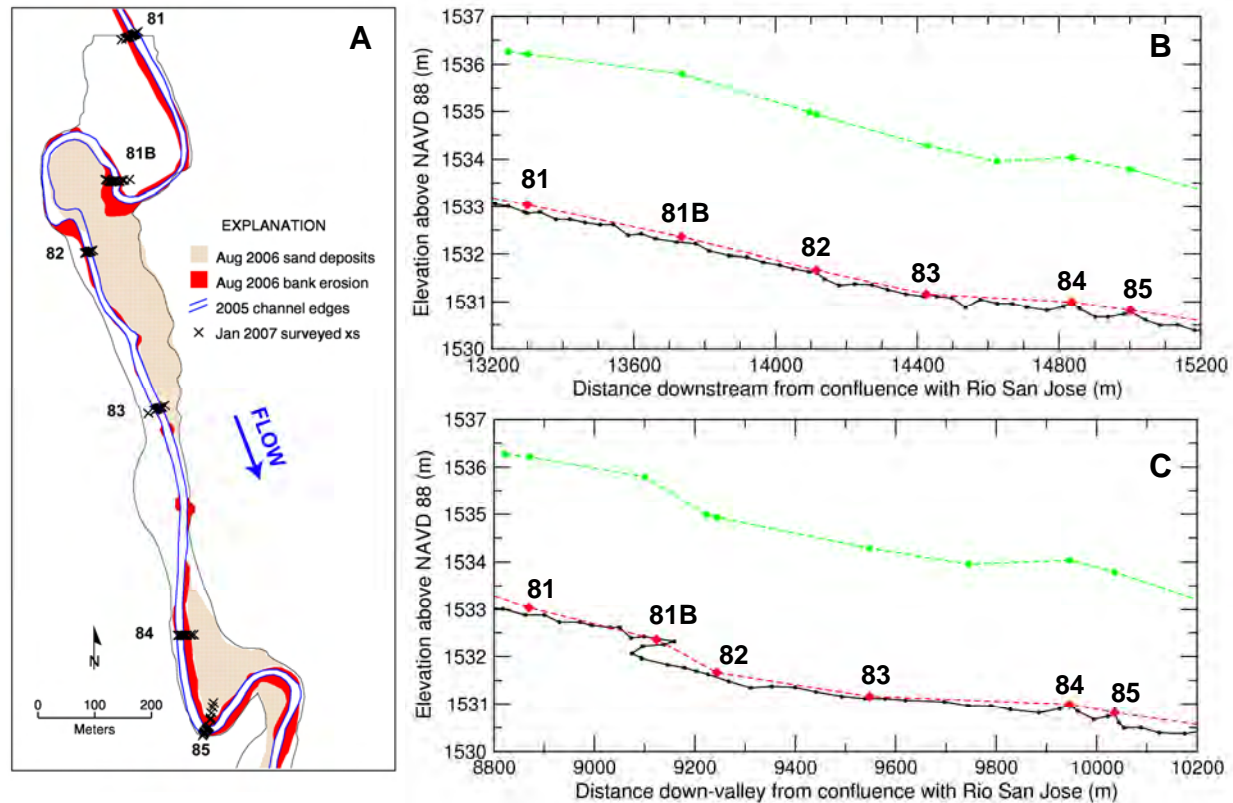


Figure 5. Map view (A) and longitudinal profiles (B and C) for the modeled channel segments. Floodplain extent, indicated by thin black lines in A, is highly variable, limited by the arroyo walls or local terraces. Longitudinal profiles from January 2007 survey data provide local floodplain (green dashed lines), thalweg (black lines) and average bed (red dashed lines) gradients for flow paths downstream following the channel (B) and directly down-valley (C).

APPLIED MODELS OF FLOW AND SEDIMENT TRANSPORT

Flow Model

This work is focused on changes in channel boundary shear stress that resulted in lateral streambank erosion and transport of sediment, dominantly sand, downstream. Therefore, the fraction of the flood peak flow within and directly above the channel (neglecting down-valley flow over the floodplain) was modeled as quasi-steady and horizontally uniform using the Kean and Smith (2004) model that explicitly calculates the effects of friction on the lateral boundaries to determine the velocity and boundary shear stress fields. This two-dimensional model for steady flow employs the ray-isovel turbulence closure of Houjou et al. (1990). The model also computes drag on woody vegetation along the channel banks, if present. In this case, it was assumed that most dead stems on the channel banks were removed prior to the peak flood flow.

Boundary shear stresses were high enough within the channel that flow was over a plane bed. Initial bed and bank roughness (z_0 ; before roughening of the upper bank due to mass failure) was estimated to be 0.0035 m. This value

was derived from a direct discharge measurement made near Bernardo on August 24, 2006, when flow was entirely within the channel and average depth of flow was 1.76 m.

Field evidence suggests that over-steepening of the channel banks led to relatively small-scale mass failures along the upper banks (Figure 6), creating drag-producing topographic features about 40 cm in height and 20 cm in width and depth. These features are superimposed on larger-scale (1-2 m) bank undulations. The rough upper bank begins about 1.4 m above the nearly flat channel bed. Lower banks were smooth in comparison, suggesting both direct fluvial erosion of the lower banks and mass failures with subsequent transport of the eroded material downstream contributed to the observed channel widening along the Rio Puerco.

Due to the lack of field measurements of upper bank topographic roughness in the eroded channel, we have estimated an average size, shape, and distribution using the features visible in Figure 6. The effective increase in total bank roughness from drag on these features was then estimated using results derived by Kean and Smith (2006b) from their measurements along the Rio Puerco of features with similar size, shape, and spacing. Mass failures along the actively eroding bank produced comparatively sharp features (low ratio of streamwise length to protrusion height). The estimated total effective roughness, $(z_0)_T$, produced by drag on a sequence of these features was 0.041 m, an order of magnitude greater than the estimated bed and initial bank roughness, $(z_0)_{sf} = 0.0035$ m.

Flow and sediment transport in the widened channel were affected by drag on the rough upper bank, which reduced the skin friction shear stress, τ_{sf} , by the shear stress due to drag on the roughness elements, τ_D . Total boundary shear stress computed by the model, $(\tau_b)_T = \rho(u_*)_T^2$, is

$$(\tau_b)_T = \tau_{sf} + \tau_D, \quad (1)$$

where $(u_*)_T = (gRS)^{1/2}$, ρ is the density of water, g is acceleration due to gravity, R is the hydraulic radius, and S is the slope. By matching the inner (near-bed) and outer velocity profiles at the average height of the roughness elements, $H = 0.40$ m, following the method of Smith and McLean (1977) and Kean and Smith (2006a), the shear stress due to skin friction, needed to compute erosion or deposition of sand, was determined by solving the equation:

$$(u_*)_{sf} / (u_*)_T = \ln\left(\frac{H}{(z_0)_T}\right) / \ln\left(\frac{H}{(z_0)_{sf}}\right) \quad (2)$$

Equation 2 was solved using the known $(z_0)_T$ and $(z_0)_{sf}$, and $(u_*)_T$ determined from the flow model-calculated boundary shear stress to find the skin friction shear stress, $\tau_{sf} = \rho(u_*)_{sf}^2$. An example is provided in the Results section.

Modeled Cases

The peak flood discharge in the modeled reach is not known. However, reach-average discharge in and directly above the channel was estimated by first applying the model to the “early flood” channel shape (Figure 3; Table 1) using the average height of the surveyed high-water marks above the channel bed, 4.2 m, to specify the stage and average slope determined from the high-water marks in the sprayed reach, 0.0021. Bed and bank roughness were set to 0.0035 m, and the channel banks were extrapolated upward to the water surface. Model-calculated discharge for this case, Case 1, was then used as the target discharge for model Cases 2 and 3.

Case 2 represents the low-gradient reach between surveyed cross-section 83, where there was little evidence of bank erosion, and cross-section 84, where the left bank (down-valley side of the channel) eroded a total of about 12 m. The widened channel shape (“eroded banks” shape of Table 1; red line in Figure 3) and average floodplain and channel bed gradient approaching cross-section 84, 0.0006, were specified. Bed roughness was set to 0.0035 m as in Case 1, and upper bank roughness was increased to 0.041 m as described above. The Kean and Smith (2004) flow model was applied, iterating on the stage, until the model-calculated discharge matched that of Case 1. Suspended sediment concentration computed for this case determined the volume concentration of sand already in suspension in the flow approaching cross-section 84.

Case 3 represents the flow conditions at the site of observed bank erosion at cross-section 84. The same channel shape and roughness parameters as used for Case 2 were specified for this case. Channel bed and floodplain gradients increased in the vicinity of cross-section 84 to an average of 0.0015. The flow model was applied for this case by again iterating on the stage to find the stage that resulted in the same discharge as Cases 1 and 2.



Figure 6. January 2007 photograph showing a segment of eroded bank with an average height of about 2.5 m. Dense, dead saltcedar stems cover the floodplain surface beyond the bank. Dimensions of upper bank topographic roughness elements were estimated from features visible in the photograph, scaled by the known bank height. (Photo by Julie Roth, Arctic Slope Regional Corp.)

Sediment Transport Model

Bed and Bank Material

Data from three long trenches excavated across the arroyo bottom between 1999 and 2001 indicate bed and bank material are relatively uniform throughout the 55-km-long arroyo reach from Hwy 6 to Bernardo (Friedman et al, 2005; unpublished data). Similarities in channel and arroyo planform geometry and the lack of substantial tributary inflow downstream from the confluence with the Rio San Jose suggest that the channel bed and bank composition throughout the sprayed reach are similar. Based on the available data, it was assumed that channel bed and banks were composed mostly of silty sands, with D_{50} in the range of fine to very fine sand. Sediment size distributions influence the concentrations of particles in suspension (Smith and McLean, 1977). We included this effect using an estimate of the bed and bank material distributions represented by 5 size classes ranging from medium silt to medium sand (Table 2). Critical shear stress for each particle size was computed using the method of Wiberg and Smith (1987). Settling velocities were computed using the method of Dietrich (1982) and adjusted for the bulk fluid density in each modeled case.

Table 2. Modeled bed material size distribution.

Sediment Size (mm)	Fraction of the bed material	$(u^*)_{cr}$ (m/s)	Clear-water settling velocity (m/s)
0.016	0.25	0.0073	0.0002
0.05	0.15	0.0087	0.0020
0.07	0.35	0.0096	0.0036
0.13	0.15	0.0113	0.0102
0.26	0.10	0.0133	0.0283

Suspended Sediment Transport

Suspended sediment concentrations were computed following the method of McLean (1992) neglecting the effects of density stratification. High concentrations of sand in suspension may create a density gradient that dampens the turbulent mixing and reduces the total volume of sand in suspension (Gelfenbaum and Smith, 1986; McLean, 1992; Wright and Parker, 2004). Gradient Richardson numbers computed for the modeled cases indicate that the flow would be stratified if it were in a much wider stream. However, in this narrow channel, secondary circulations caused by slumping sediment (grain-flow process) or slumped blocks of sediment contribute to uniform mixing across the channel. Convective accelerations resulting from a meandering thalweg also contribute to cross-channel mixing. Therefore, we have neglected effects of density stratification and computed suspended sediment profiles using the Rouse (1937) formula, which produces an upper bound for the estimation of suspended sand transport rates.

Concentrations of each sediment size in suspension were computed from the specified concentration of sediment in the bed and the transport stage, T_* , which is the ratio of shear stress due to skin friction, τ_{sf} , to the critical shear stress, τ_{cr} , for each particle size. As noted by Topping et al. (2007), the fractional area of the bed over which sand is available for transport affects the concentration of sand in suspension. We computed suspended sediment concentrations assuming sand was available for transport over the bed fraction of the wetted perimeter (Table 1). The concentration of sediment in the bed, C_b , 0.65 (assuming 35% porosity), was then multiplied by the bed fraction of the perimeter (0.44 for Case 1; 0.60 for Cases 2 and 3; Table 1) to estimate the net concentration of sediment available for transport. The reference concentration, C_a , was then computed following the method of Smith and McLean (1977), as

$$C_a = \frac{\gamma_0 C_b (T_* - 1)}{1 + \gamma_0 (T_* - 1)}, \quad (3)$$

where $\gamma_0 = 0.004$ (P. L. Wiberg, as reported by McLean, 1992). Transport stage varied among the modeled cases, so that the reference concentration for each particle size was different for each case.

RESULTS AND DISCUSSION

Model-Calculated Flow

Model-calculated discharge for all three cases was about 120 m³/s. Cross-sectional geometries for the three cases at the calculated flood-flow stages are shown in Table 3. Hydraulic radii shown in Table 3 include extrapolation of the wetted perimeter upward to the water surface. The large increase in slope from Case 2 to Case 3 resulted in a large decrease (>1 m) in the calculated flow stage. Model-calculated velocity and boundary shear stress distributions for each case (Table 4) were used to compute suspended sediment concentration profiles.

Table 3. Modeled channel geometries at the flood-flow stages.

Model Case	Stage (m)	Top width (m)	XS area (m ²)	Hydraulic radius (m)	Average depth (m)	Slope
Case 1	4.20	15.5	45.8	2.49	2.96	0.0021
Case 2	4.50	19.6	70.2	3.03	3.59	0.0006
Case 3	3.34	18.0	48.4	2.38	2.69	0.0015

Table 4. Model-calculated flow parameters.

Model Case	Discharge (m ³ /s)	Mean velocity (m/s)	Mean model-calculated τ_b (N/m ²)	Manning's n	Froude number
Case 1	120.5	2.63	49.8	0.031	0.53
Case 2	120.2	1.71	17.7	0.030	0.31
Case 3	120.0	2.48	34.0	0.028	0.51

Calculated Suspended Sediment Concentrations

Computed sand concentrations and volume fluxes (Table 5) are maximum values assuming sand is available for transport across the bed. At any particular location, the available sand supply likely varied as a function of time, affected by the rates and volumes of bank mass failures. Therefore, the computed concentrations are considered averages in time and space. Calculated suspended sediment concentrations are an order of magnitude greater than measured volume concentrations from samples collected near Bernardo on August 4, 2006, 0.0128 (34,000 mg/L) and on August 10, 0.0063 (16,700 mg/L) during the peak flood flow (U.S. Geological Survey (USGS), Water-Quality (QW) Data for New Mexico, available at <http://waterdata.usgs.gov/nm/nwis/qw/>). However, these samples were collected at a site about 81 km downstream from the eroded reach (sediment size distributions in these samples were not provided). Based on observations from the January 2007 field survey and post-flood imagery, we infer that all sand eroded from the banks in the sprayed reach was deposited on the floodplain or channel bed within about 10 km down-valley from Hwy 6. Therefore, sediment in suspension near Bernardo was likely finer than sand and carried as wash load (Graf, 1984).

Table 5. Computed suspended sediment concentrations and volume fluxes.

Model Case	Vertically averaged volume concentration		Volume flux (m ³ /s)	
	Total sediment	Total sand	Total sediment	Total sand
Case 1	0.1718	0.0919	20.7	11.1
Case 2	0.1186	0.0593	14.3	7.1
Case 3	0.1946	0.1021	23.4	12.3

The computed sediment concentrations for the August 2006 flood in the eroded reach are similar to those measured in samples collected at the streamflow-gaging station near Bernardo in the 1950s (USGS, QW Data for New Mexico, available at <http://waterdata.usgs.gov/nm/nwis/qw/>) prior to stabilization of the channel and floodplain by establishment of dense saltcedar stands along the lower Rio Puerco (Elliott et al., 1999; Friedman et al., 2005). For example, comparable volume concentrations were measured in August 1952, when the total suspended sediment concentration was 0.1238 (328,000 mg/L) and the volume concentration of sand was 0.0483 (39% of the sampled sediment). Samples collected in September 1950 included total volume concentrations as high as 0.1445 (383,000 mg/L) with a sand concentration of 0.0578 (40% of the sample).

Streamwise velocity of the suspended sand is assumed to be the same as the mean flow velocity (Graf, 1984); therefore, the volume flux was computed by multiplying the volume concentration of sand by the flow discharge. Computed volume concentrations and volume fluxes of sand demonstrate the effects of converging flow in the channel segment approaching cross-section 83 and diverging flow in the vicinity of cross-section 84. Decreasing slope and total boundary shear stress approaching cross-section 83 forced the deposition of sand on the floodplain (Figure 5) and possibly on the channel bed. Shear stress remained relatively constant in both the channel and floodplain flow through an approximately 200-m-long segment downstream from cross-section 83, as indicated by limited channel bank erosion and sand deposition on the floodplain (Figure 5). Near cross-section 84, the downstream channel flow diverged from the down-valley flood flow along a bend in the down-valley axis, and both channel bed and floodplain slopes increased. The resulting 5.2-m³/s increase in the volume flux of sand from Case 2 to Case 3 provides an indication of the bank erosion rate in the vicinity of cross-section 84. The total volume of bank sediment eroded from a 140-m-long channel segment including cross-section 84 was about 2,617 m³, and the time required to erode that volume at a rate of 5.2 m³/s was about 8.4 minutes.

Bank Shear Stress Distribution

Modeled boundary shear stress distributions along the channel banks (Figure 7; Table 6) demonstrate both the effects of form drag in decreasing the skin friction shear stress, τ_{sf} , and the effects of increasing bed gradient in eroding the bank. Erosion of sediment requires an increase in τ_{sf} , and the magnitude of the increase determines the potential erosion rate. We know the left channel bank eroded about 12 m in the vicinity of cross-section 84 during the August 2006 flood. Skin friction shear stresses computed using equation (2) and model-calculated $(\tau_b)_T$ along the

bank at a height 2 m above the bed are 77% less than the total boundary shear stress and 67% (Case 2) and 57% (Case 3) less than the local depth-slope product, ρghS (Table 6).

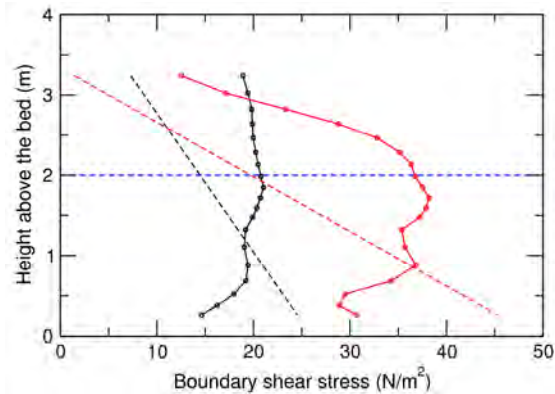


Figure 7. Model-calculated total boundary shear stress distributions along the bank for Cases 2 (black solid line) and 3 (red solid line). The dashed lines represent the depth-slope product for each case. Reference concentrations for fine sand ($d = 0.13$ mm) were computed at a bank height of 2 m (blue dashed line), where the model-calculated total boundary shear stresses exceeded the local depth-slope product by 43% (Case 2) and 86% (Case 3).

Table 6. Computed reference concentrations at a point along the bank 2 m above the bed.

Model Case	Height above the bed (m)	Model-calculated $(\tau_b)_T$ (N/m ²)	Local ρghS (N/m ²)	τ_{sf} (N/m ²), with form drag removed	T^*	C_a ($d = 0.13$ mm)
Case 2	2.0	20.8	14.5	4.80	37.8	0.00751
Case 3	2.0	36.7	19.7	8.53	67.2	0.01224

Reference concentrations, C_a , for the bed material size representing D_{84} , 0.13 mm (15% of the bed material), computed from the skin friction shear stresses (Table 6) show the effect of the increasing τ_{sf} resulting from the increase in bed gradient. Critical shear stress for 0.13 mm sand, used to compute the transport stage, is 0.127 N/m² (computed using the method of Wiberg and Smith, 1987). The model-calculated boundary shear stress is relatively constant for the low-gradient and high stage Case 2, averaging about 19 N/m² along the bank above about 0.7 m (Figure 7). An increase in the water-surface slope to 0.0015 (Case 3) increased the shear stress along the bank and the transport stage by about 78%. As a result, the reference concentration for 0.13 mm sand in suspension (Table 6) and the potential sand transport rate for this size increased by about 63%.

CONCLUSIONS

Computed boundary shear stress distributions and volume fluxes of sand for the three modeled cases demonstrate the influence of local geomorphic setting, including floodplain slope and orientation of the channel centerline relative to the down-valley axis, on the capacity of the August 2006 peak flood flow to erode the channel banks. Model-calculated boundary shear stress distributions indicate steepening of the channel banks through mass failures and direct fluvial erosion reduced the shear stress at the bank toe and the erosion rate as the channel widened during the flood. These results demonstrate the importance of being able to compute the boundary shear stress distribution along the channel bank rather than having to rely on the depth-slope product to estimate erosion and sediment transport.

REFERENCES

Barz, D., Watson, R.P., Kanney, J.F., Roberts, J.D., and Groeneveld, D.P. (2009). "Cost/benefit considerations for recent saltcedar control, Middle Pecos River, New Mexico," *Environmental Management*, 43, pp 282-298.

- Bryan, K. and Post, G.M. (1927), "Erosion and control of silt on the Rio Puerco, New Mexico. Report to the Chief Engineer, Middle Rio Grande Conservancy District, Albuquerque, NM.
- Cleverly, J.R., Dahm, C.N., and Coonrod, J.E.A. (2006), "Groundwater, vegetation, and atmosphere: Comparative riparian evapotranspiration, restoration, and water salvage," USDA Forest Service Proc. RMRS-P-42CD, pp 75-80.
- Dietrich, W.E. (1982). "Settling velocity of natural particles," *Water Resources Research*, 18(6), pp 1615-1626.
- Elliott, J.G., Gellis, A.C., and Aby, S.B. (1999). "Evolution of arroyos: incised channels of the southwestern United States," in Darby, S.E. and Simon, A., (eds.), *Incised River Channels*, John Wiley and Sons, New Jersey, pp 153-185.
- Friedman, J.M., Vincent, K.R., and Shafroth, P.B. (2005). "Dating flood-plain sediments using tree-ring response to burial," *Earth Surf. Processes Landforms*, 30(9), pp 1077-1091.
- Gelfenbaum, G. and Smith, J.D. (1986). "Experimental evaluation of a generalized suspended-sediment transport theory," in Knight, R.J. and McLean, J.R., (eds.), *Shelf Sands and Sandstones*. Canadian Society of Petroleum Geologists, Memoir II, pp 133-144.
- Graf, W.H. (1984). *Hydraulics of Sediment Transport*. Water Resources Publications, LLC., Highlands Ranch, Colorado.
- Griffin, E.R., Kean, J.W., Vincent, K.R., Smith, J.D., and Friedman, J.M. (2005). "Modeling effects of bank friction and woody bank vegetation on channel flow and boundary shear stress in the Rio Puerco, New Mexico," *Journal of Geophysical Research*, 110, F04023, doi:10.1029/2005JF000322.
- Houjou, K., Shimizu, Y., and Ishii, C. (1990). "Calculation of boundary shear stress in open channel flow," *Journal of Hydroscience and Hydraulic Engineering*, 8, pp 21-37.
- Kean, J.W. and Smith, J.D. (2004). "Flow and boundary shear stress in channels with woody bank vegetation," in Bennett S, Simon A (eds). *Riparian Vegetation and Fluvial Geomorphology*. Water Science and Applications, vol. 8. American Geophysical Union, Washington, D.C., pp 237-252.
- Kean, J.W. and Smith, J.D. (2006a). "Form drag in rivers due to small-scale natural topographic features: 1. Regular sequences," *Journal of Geophysical Research*, 111, F04009, doi:10.1029/2006JF000467.
- Kean, J.W. and Smith, J.D. (2006b). "Form drag in rivers due to small-scale natural topographic features: 2. Irregular sequences," *Journal of Geophysical Research*, 111, F04010, doi:10.1029/2006JF000490.
- Love, D.W. (1986), "A geological perspective of sediment storage and delivery along the Rio Puerco, central New Mexico," in Hadley, R.F., ed., *Drainage basin sediment delivery*, IAHS Publication 159, International Association of Hydrological Sciences Press, Wallingford, UK, pp 305-322.
- McLean, S.R. (1992). "On the calculation of suspended load for noncohesive sediments," *Journal of Geophysical Research*, 97(C4), pp 5759-5770.
- National Climate Data Center (2006). *Record of Climatological Observations, 24-hour Precipitation Totals and Hourly Precipitation Data, New Mexico*, 56(8), National Oceanic and Atmospheric Administration, Asheville, North Carolina.
- National Weather Service, Advanced Hydrologic Prediction Service (2006). "About the precipitation analysis pages," accessed June 25, 2009 at <http://water.weather.gov/>.
- National Weather Service Weather Forecast Office, Albuquerque, New Mexico (2006). "August 2006 weather highlights for New Mexico," accessed online June 25, 2009 at <http://www.srh.noaa.gov/abq/climate/Monthlyreports/August2006/>.
- Rouse, H. (1937). "Modern conceptions of the mechanics of fluid turbulence." *Trans. Am. Soc. Civ. Eng.*, 102, pp 463-543.
- Shafroth, P.B., Cleverly, J.R., Dudley, T.L., Taylor, J.P., Van Riper III, C., Weeks, E.P., and Stuart, J.N. (2005), "Control of Tamarix in the western United States: Implications for water salvage, wildlife use, and riparian restoration," *Environmental Management*, 35(3), pp 231-246.
- Smith, J.D. and McLean, S.R. (1977). "Spatially averaged flow over a wavy surface," *Journal of Geophysical Research*, 82(12), pp 1735-1746.
- Smith, J.D. (2007). "Beaver, willow shrubs and floods," in Johnson EA, Miyanishi K, eds., *Plant Disturbance Ecology: The Process and the Response*. Elsevier Academic Press, Burlington, MA, pp 603-672.
- Tiffin, J. (2006). "Storm sends flood waters into Cubero across I-40," *Gallup Independent Web Edition*, August 5, 2006, accessed July 16, 2009 at <http://www.gallupindependent.com/>.
- Topping, D.J., Rubin, D.M., and Melis, T.S. (2007). "Coupled changes in sand grain size and sand transport driven by changes in the upstream supply of sand in the Colorado River: Relative importance of changes in bed-sand grain size and bed-sand area," *Sedimentary Geology*, 202, pp 538-561.
- Vincent, K.R., Friedman, J.M., and Griffin, E.R. (2009). "Erosional consequence of saltcedar control," *Environmental Management*, 44, pp 218-227.
- Western Regional Climate Center (2009). *Monthly Total Precipitation, Period of Record Climate Summary*, accessed online November 6, 2009 at <http://www.wrcc.dri.edu/>.
- Wiberg, P.L. and Smith, J.D. (1987). "Calculations of the critical shear stress for motion of uniform and heterogeneous sediments," *Water Resources Research*, 23(8), pp 1471-1480.
- Wilcox, B.P., Owens, M.K., Dugas, W.A., Ueckert, D.N., and Hart, C.R. (2006), "Shrubs, streamflow, and the paradox of scale," *Hydrological Processes*, 20, pp 3245-3259.
- Wright, S. and Parker, G. (2004). "Density stratification effects in sand-bed rivers," *Journal of Hydraulic Engineering*, 130(8), pp 783-795.